Journal of Materials Chemistry A

Accepted Manuscript

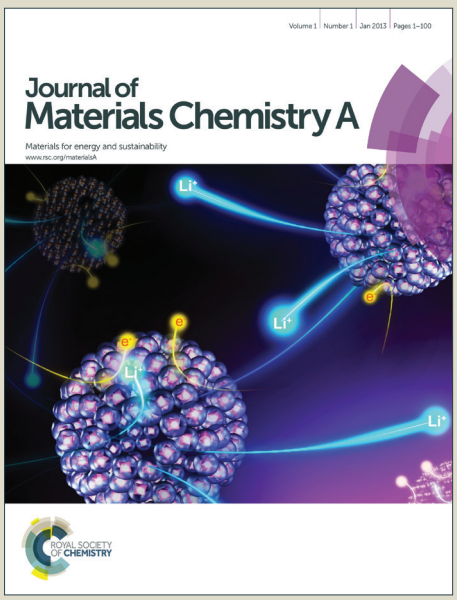

ROYAL SOCIETY OF CHEMISTRY

www.rsc.org/materialsA

Tailoring Chemical Expansion by Controlling Charge Localization:

In Situ X-ray Diffraction and Dilatometric Study of (La,Sr)(Ga,Ni)$O_{3-\delta}$ Perovskite

Nicola H. Perry[a,b], Sean R. Bishop[a,b], and Harry L. Tuller[a,b]

[a.] International Institute for Carbon-Neutral Energy Research (I2CNER), Kyushu University, 744 Motooka, Nishi-ku Fukuoka 819-0395, Japan

[b.] Department of Materials Science and Engineering, Massachusetts Institute of Technology, 77 Massachusetts Avenue, Cambridge, MA 02139, U.S.A.

Table of Contents Graphic & Text

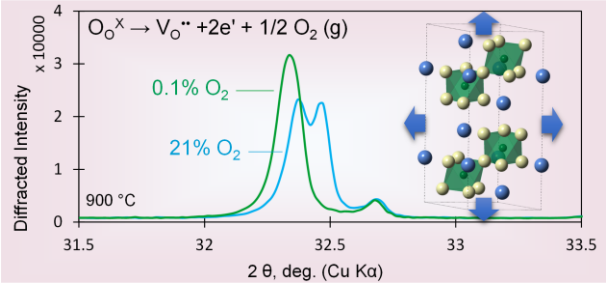

Charge delocalization, experimentally controlled, was shown to correlate with reduced chemical expansion, for enhanced durability of energy-related perovskites, supporting prior theoretical predictions. Subtle structural changes during expansion were also observed.

Abstract

Large coupling of oxygen content and lattice dilation, known as chemical expansion, deleteriously impacts durability of non-stoichiometric active oxides in energy conversion and storage devices. In this work, the role of charge localization on multivalent cations during reduction was experimentally probed using $La_{0.9}Sr_{0.1}Ga_{1-x}Ni_xO_{3-\delta}$ (LSGN; x = 0.05, 0.1, and 0.5) to test prior theoretical predictions of decreased chemical expansion upon decreasing charge localization. Increasing Ni content in LSGN resulted in a decrease in the coefficient of chemical expansion, consistent with expected charge de-localization as LSGN transitions from polaron hopping to metallic conduction, as demonstrated in prior electrical studies. Dilatometry and thermogravimetry showed that samples with more Ni underwent larger changes in oxygen

content and consequently expanded more, though the normalized expansion for a given stoichiometry change (the coefficient of chemical expansion) was less. *In situ* X-ray diffraction revealed an increase of crystal symmetry with decreasing oxygen partial pressure and/or increasing temperature, consistent with expected changes in Ni and anion radii and demonstrating the interplay between chemical expansion and crystal structure. The smaller-than-expected magnitude of the change in chemical expansion coefficient with charge delocalization, compared to prior theoretical predictions, suggests that other factors, such as structural changes and the nature of the multivalent cation, likely also contribute. Finally, the effective radius of an oxygen vacancy (smaller than an oxide ion) as well as the change in size of Ni with charge de-localization, was estimated.

Introduction

Chemical expansion (ε_C) is the lattice dilation of a material in response to a composition change[1,2,3]. A gradual chemical expansion with continuous change in stoichiometry has recently been referred to as "stoichiometric expansion," as opposed to the often larger expansions accompanying changes in phase with composition, i.e., "phase change expansion."[1] In the context of non-stoichiometric oxides, this expansion typically accompanies oxygen loss ($\Delta\delta$) in, e.g., perovskite oxides of general formula $ABO_{3\pm\delta}$. In a manner analogous to thermal expansion, it can be represented as

$$\varepsilon_C = \alpha_C \Delta\delta \qquad (1)$$

where α_C is the coefficient of chemical expansion (CCE). Arising in part from their ability to sustain significant and variable values of δ, such non-stoichiometric oxides often exhibit mixed ionic and electronic conductivity. For this reason they are widely incorporated in electrochemical devices, e.g., as solid oxide fuel/electrolysis cell electrodes, where they exhibit enhanced reaction kinetics and enlarged active areas compared to conventional two-phase composite electrodes[4]. However, variations in temperature and/or oxygen partial pressure during fabrication or operation result in changes in oxygen stoichiometry in these materials, with consequent dimensional changes. The resulting stresses[5,6,7] can lead to cracking or

delamination[8,9], either in a monolithic material with non-uniform stoichiometry or at the interfaces of dissimilar materials. Such chemical expansion-induced failure represents a widespread challenge impacting many energy conversion and storage devices that incorporate or release ions, including hydrogen storage materials and battery materials[1]. In order to extend device lifetime, fundamental studies of the factors governing chemical expansion in oxides need to be pursued.

The process of reduction of a non-stoichiometric perovskite, with a multivalent B-site cation, can be expressed in Kröger-Vink notation as:

$$2B_B^x + O_O^x \rightarrow 2B_B' + V_O^{\cdot\cdot} + \frac{1}{2}O_2(g) \qquad (2)$$

The formation of a charged oxygen vacancy yields two electrons for charge neutrality, which can be localized on two multivalent B-site cations, effectively lowering their valence state (e.g., from 3+ to 2+). Marrocchelli *et al.*[10] described the CCE as a sum of contributions originating from the metal cations (α_M) and from the anions/ anion vacancies (α_V):

$$\alpha_C = \alpha_M + \alpha_V \qquad (3)$$

In that work on fluorite-structured oxides, α_M was found to be a positive term, owing to expansion of multivalent cations as they lower their valence state, while α_V was negative, owing to contractive relaxations around oxygen vacancies described by the empirical parameter "oxygen vacancy radius," which is smaller than the radius of an oxide ion. In order to minimize chemical expansion, strategies to further shrink the oxygen vacancy radius, by changing the host cation, were pursued[11]. As investigated in the present work, one can also decrease the expansion of the multivalent cation as a means of reducing the overall CCE. Accordingly, recent density functional theory (DFT) calculations by Marrocchelli *et al.*[12] highlighted the potentially key role that charge localization on multivalent cations (Ce in CeO_2 and $BaCeO_3$) could play in both the fluorite and perovskite structures. In that work a reduction of over 70% in CCE was calculated upon artificially delocalizing the charge on Ce.

In the present work we test this theoretical prediction experimentally to understand the contribution of charge localization in perovskite CCEs. Additionally, by way of high temperature X-ray diffraction (HTXRD), we explore the impact δ has on crystal symmetry. In practice, charge delocalization is difficult to achieve in the Ce-based systems discussed above; experimentally, the electronic conductivity in CeO_2 is governed by polaron hopping[13], indicative of charge localization on $Ce^{4+/3+}$, and in $BaCeO_3$ very low oxygen partial pressures and high temperatures are required for reduction of Ce^{4+} to Ce^{3+} [14]. By contrast, the perovskite (La,Sr)(Ga,Ni)$O_{3-\delta}$ (LSGN), containing multivalent $Ni^{3+/2+}$ and a high Ni solubility, given the similar ionic radii to Ga^{3+}, represents a model system for such studies. Exhibiting high ionic and electronic conductivities, in addition to chemical and mechanical compatibility with (La,Sr)(Ga,Mg)$O_{3-\delta}$ electrolytes, LSGN and La(Ga,Ni)$O_{3-\delta}$ (LGN) have been investigated previously as promising solid oxide fuel cell cathodes[15,16], oxygen separation membranes[17], and natural gas conversion membranes[18,19]. Measurements of LSGN by Long *et al.*[20] demonstrated a transition from low, thermally-activated electrical conductivity to conductivity orders of magnitude higher and weakly decreasing with temperature, upon increasing the Ni concentration, x in $La_{0.9}Sr_{0.1}Ga_{1-x}Ni_xO_{3-\delta}$, from 0.05 to 0.5. In combination with oxygen partial pressure-dependent measurements, the behavior was consistent with a transition from ionic, to electronic polaron hopping, to metallic conductivity controlled by phonon scattering with increasing Ni content, which may be explained by the widening of the Ni 3d impurity band and corresponding delocalization of charge as the Ni concentration increases. Similar electrical behavior has been observed in LGN[16], and, in other perovskites with high Ni content, such as $LaNiO_3$ (with Ni in the 3+ state), metallic behavior has been attributed to delocalized Ni 3d and O 2p valence states.[21] Therefore, in addition to its theoretically predicted correlation to lower CCE values, charge delocalization beneficially enhances the electronic conductivity, which is desirable for improved current collection and thus reduced ohmic losses in energy conversion devices. The addition of Ni, leading to charge delocalization, also beneficially enhances the ionic conductivity at lower oxygen partial pressures, where it dominates the total conductivity[20]. In the present work the corresponding change in CCE with Ni content is studied by *in situ* X-ray diffraction, thermogravimetry, and dilatometry under cathodic conditions, building upon our preliminary work on LSGN [22].

Results

Crystal Structure During Expansion

X-ray diffraction revealed the presence of minor phases in all samples: $(Sr,La)_2(Ga,Ni)_3O_{7-\delta}$ in the samples with low Ni content (x = 0.05, 0.1) and $(Sr,La)_2(Ga,Ni)O_{4-\delta}$ with trace NiO in the sample with higher Ni content (x = 0.5). Such results are consistent with those reported by Colomer and Kilner[23], who observed $SrLa(Ga,Ni)_3O_{7-\delta}$ in an x = 0.1 sample and $SrLa(Ga,Ni)O_{4-\delta}$ in an x = 0.2 sample. The presence of minor impurity phases indicates that the major perovskite phases may deviate slightly from the nominal sample compositions. Regarding the primary LSGN perovskite phase, addition of Ni at x = 0.1 and x = 0.5 resulted in stabilization of the rhombohedral (R-3c) structure at room temperature in agreement with prior reports[20,23], whereas the x = 0.05 specimen was orthorhombic (Pbnm) at room temperature, similar to undoped $LaGaO_{3-\delta}$[24]. With increasing temperature and/or decreasing oxygen partial pressure, shifts in peak positions (as expected from thermal and chemical expansion) and changes in symmetry were observed in the perovskite phase.

One way to visualize such changes is to view the most intense peak(s) in the range 32-33° 2θ (for Cu Kα); for the orthorhombic phase a triplet (200/112/020) is present, whereas for the rhombohedral phase a doublet (110/104) is found. Figure 1 shows the change in peak shapes and locations as a function of Ni concentration, temperature, and oxygen partial pressure, with $K\alpha_2$ contributions removed for clarity.

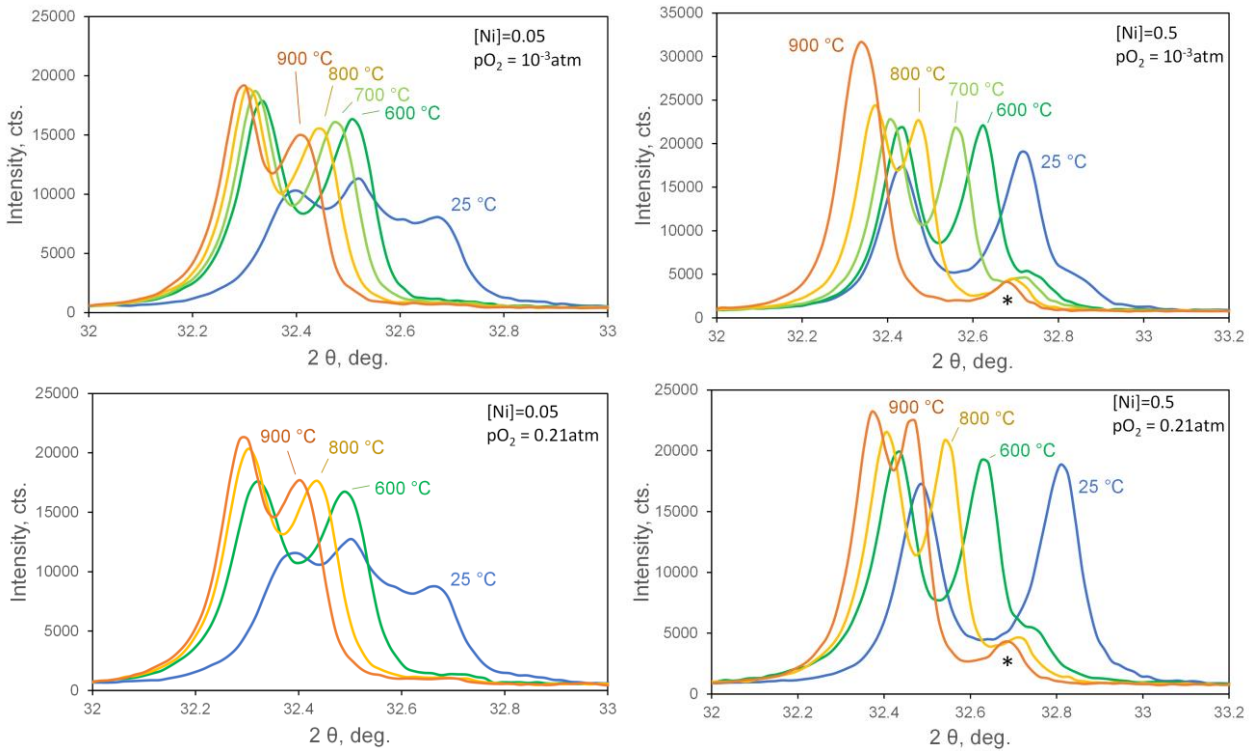

Figure 1. Highest intensity XRD peaks corresponding to the perovskite phase (except the small peak/ shoulder marked with an asterisk, which is the $(Sr,La)_2(Ga,Ni)O_{4-\delta}$ phase), as a function of Ni content, temperature, and oxygen partial pressure. The measurements shown for 25 °C were taken after cooling in the gas atmosphere indicated.

The x = 0.05 sample appears rhombohedral at elevated temperatures, which is consistent with the reported transition from orthorhombic to rhombohedral structure for undoped $LaGaO_{3-\delta}$ at ~145 °C[24]. With increasing temperature, for both samples, the two rhombohedral peaks approach each other, suggesting an increase in symmetry toward the cubic Pm-3m structure. The same transition towards increasing symmetry can be observed upon decreasing the oxygen partial pressure, and for the x = 0.5 sample at 900 °C and $pO_2 = 10^{-3}$ atm the two rhombohedral peaks have merged into one indistinguishable peak, almost reaching the Pm-3m structure. (The smaller peak that becomes visible near 32.7°, indicated by an asterisk, is from the $(Sr,La)_2(Ga,Ni)O_{4-\delta}$ phase; it does not change location upon changing oxygen partial pressure and is not consistent with any other perovskite phase that fits the remaining peaks.)

In addition, the peaks move to lower angles with increasing temperature and decreasing oxygen partial pressure, consistent with thermal and chemical expansion. Note that in the case of x = 0.05 only a very small change in peak position and shape is observed upon decreasing the oxygen partial pressure (more apparent at high angle peaks, not shown), suggesting very limited chemical expansion over this oxygen partial pressure range (0.21 to 10^{-3}atm). (For this reason, a wider range of oxygen partial pressures was employed to study the macroscopic chemical expansion of this composition using dilatometry.) No shift in peak positions (even for high angle peaks) with changes in oxygen partial pressure was observed for the secondary phases, suggesting a negligible contribution to chemical expansion from the minor phases. Figure 2 (parts a and b) shows lattice parameters vs. temperature by fitting the data to the R-3c structural model, for the two oxygen partial pressures and two compositions, x = 0.05 and x = 0.5. (Note the data at 25 °C for x = 0.05 are approximate pseudo-rhombohedral lattice parameters for that orthorhombic structure.) Generally the sample with a lower Ni concentration (x = 0.05) exhibited a larger unit cell than that of x = 0.5.

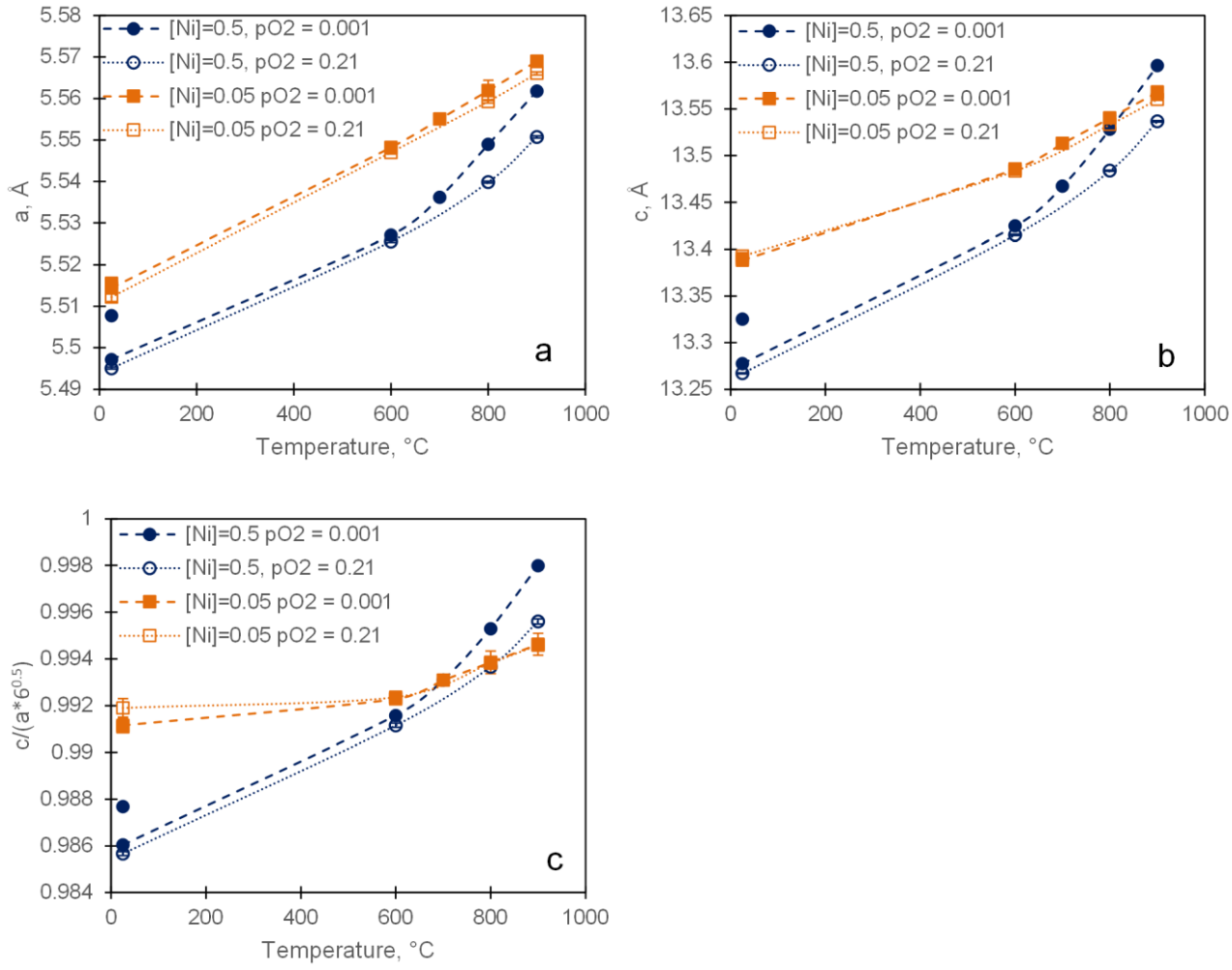

Figure 2. Lattice parameters (figs. a-b) and a corresponding measure of symmetry (fig. c) obtained for fitting in situ XRD patterns according to R-3c symmetry, during heating and cooling. (The two values at room temperature shown for each condition indicate parameters before and after heating in the atmosphere indicated. Parameters after cooling in 0.001 atm O_2 were larger than the initial value.) Dashed lines are a guide for the eye, fit to the data measured during heating.

In figure 2c, a measure of structural symmetry, $c/(a*6^{0.5})$, is shown for the two samples in the different oxygen partial pressure atmospheres. Values approaching 1 indicate increasing crystal symmetry toward the cubic structure, which is apparent for increases in temperature for both samples and for decreasing oxygen partial pressure for the x = 0.5 sample. Smaller changes in symmetry for the x = 0.05 sample may, to some

extent, reflect the smaller change in oxygen stoichiometry, as expected on the basis of the lower Ni content and shown by the thermogravimetric analysis, below.

The expansion upon increasing temperature from 25 to 900 °C in air was consistent with reported values[20] and was slightly anisotropic; for x = 0.05 *a* increased 0.9±0.1% while *c* increased 1.2±0.1%, and for x = 0.5 *a* increased 1.0±0.1% while *c* increased 2.0±0.1%. Changes in profile-fitted lattice parameters with respect to oxygen partial pressure were comparable to the error bars for x = 0.05, and therefore quantification of chemical expansion from XRD results was not possible for that composition. For the x = 0.5 sample the chemical expansion over this oxygen partial pressure range (0.21 to 0.001 atm) was much larger. Like the thermo-chemical expansion during heating, this purely chemical expansion was also anisotropic: 0.16% in *a* vs. 0.33% in *c* at 800 °C and 0.20% in *a* vs. 0.40% in *c* at 900 °C (or 0.22% in the pseudo-cubic lattice parameter at 800 °C and 0.28% at 900 °C). These values appear consistent with those measured by dilatometry, as shown below, although a precise comparison cannot be made as the oxygen partial pressure range of the XRD measurements is larger than that used in the dilatometric measurements (for x = 0.5). Similar anisotropic expansion and increasing symmetry with increasing temperature and/or decreasing oxygen partial pressure have been reported previously for the related perovskites (La,Sr)$FeO_{3-\delta}$[25] and (La,Sr)$CoO_{3-\delta}$[26].

Macroscopic Expansion

Moving now to the corresponding macroscopic study of expansion using dilatometry, examples of the change in oxygen non-stoichiometry (for the x = 0.5 sample, a) and expansion (for the x = 0.05 sample, b) measured as a function of time at 900 °C are plotted in figure 3. As described in the experimental section, slight irreversible weight loss is noted in the TGA data at the two lowest oxygen partial pressures; this was corrected for by a linear offset with time in the data analysis. Similarly the drift in measured sample position over time was corrected in the analysis of equilibrium strain.

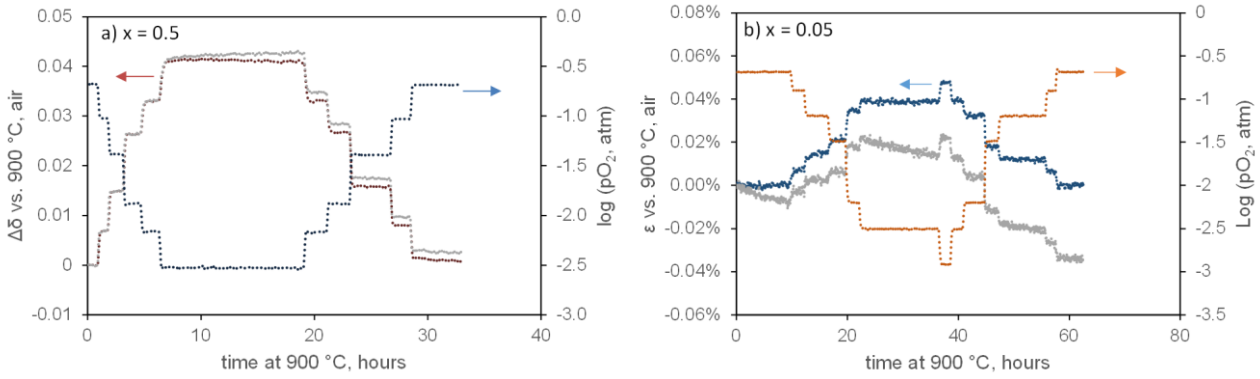

Figure 3. Examples of oxygen non-stoichiometry changes (a) and expansion (b) in response to oxygen partial pressure changes as a function of time at 900 °C for two compositions. Corrections for irreversible weight loss (a) and instrument drift (b) are also shown.

Equilibrium values of changes in non-stoichiometry as a function of oxygen partial pressure at 800 °C are shown in figure 4 for the three compositions; note that the absolute non-stoichiometry (δ) at the reference state (air) is likely different for each sample.

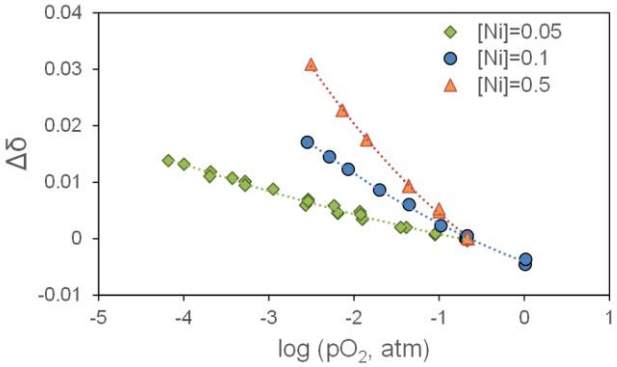

Figure 4. Oxygen non-stoichiometry change vs. oxygen partial pressure for three compositions at 800 °C.

Data measured initially in decreasing pO_2 steps, then subsequently in increasing pO_2 steps, are shown on the plot. (For x = 0.05 two separate runs were conducted over different ranges of oxygen partial pressure, so there are two forward and two reverse sweeps.) Overlap in the forward and reverse measurements (after correction for x = 0.5) indicates good reversibility. The change in non-stoichiometry over a given oxygen partial pressure range increases with increasing Ni concentration, consistent with the defect reaction in

equation 2, where the formation of oxygen vacancies is charge-compensated by reduction of the B-site cation. Corresponding equilibrium values of the relative expansion as a function of oxygen partial pressure at 800 °C are shown in figure 5; again, note that the absolute sample length at the reference state (air) is likely different for each sample.

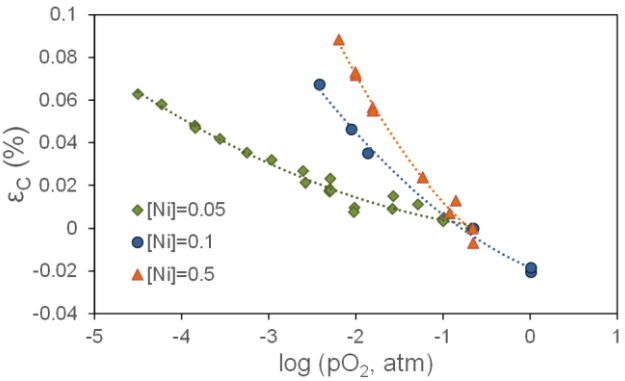

Figure 5. Isothermal expansion at 800 °C vs. oxygen partial pressure for three compositions.

Again, measurements initially in decreasing pO_2 and then in increasing pO_2 are all shown; the reasonable agreement shows reversibility. Quadratic fits to the data, used to interpolate values of ε are also indicated on the plot. The larger expansion observed for higher Ni concentrations (over a given oxygen partial pressure range) is consistent with the larger change in non-stoichiometry for those samples. The next step is to normalize the expansion to the change in non-stoichiometry for each sample. The non-stoichiometry data from figure 4 can be combined with interpolated values of ε from figure 5 at the same oxygen partial pressures to yield figure 6, which shows expansion as a function of change in non-stoichiometry at 800 °C.

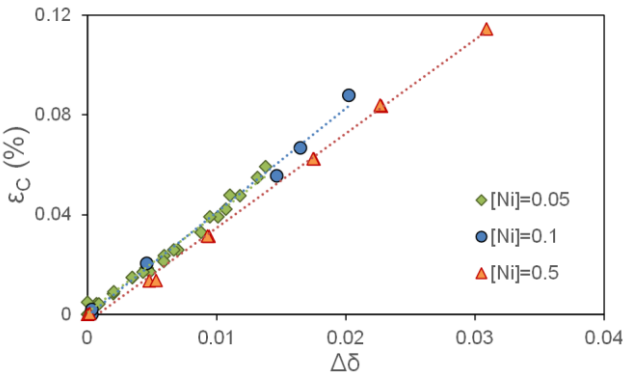

Figure 6. Isothermal chemical expansion (from the fitting in figure 5, as described in the text) vs. change in oxygen non-stoichiometry at 800 °C. Dashed lines represent linear fits to the data.

Per equation 1, the slopes of this plot are the CCEs for each sample at this temperature. A summary of all CCE values determined in this work (some at other temperatures) is given in Table I. Data used in the determination of CCEs at 700 °C and 900 °C is included as supplementary material. At 800 °C the CCE value of the x = 0.5 sample is ~5-10% lower than those of the samples with low Ni content (x = 0.05, x = 0.1) and at 900 °C it is ~20% lower than the x = 0.05 sample. These results are consistent with the larger expected CCE for a higher degree of charge localization.

Table I: CCE values in relatively high pO_2 conditions (>10^{-5} atm) determined at various temperatures for samples with different Ni contents (x).

Temperature, °C	x in $La_{0.9}Sr_{0.2}Ga_{1-x}Ni_xO_{3-\delta}$	CCE
700	0.5	0.034 ± 0.002
800	0.05	0.040 ± 0.001*
	0.1	0.042 ± 0.002
	0.5	0.0377 ± 0.0006
900	0.05	0.049 ± 0.002
	0.5	0.0408 ± 0.0005

* Note this value was determined over a wider oxygen partial pressure range.

Discussion

Origins of Structural Changes

It is clear from the *in situ* XRD results that, at a crystal structure level, thermochemical expansion and Ni substitution in LSGN involve not only changes in unit cell volume but also changes in crystal symmetry. In the perovskite structure, the larger A-site cations occupy spaces between corner-sharing BO_6 octahedra. Deviations from cubic symmetry may involve octahedral distortion (i.e., Jahn-Teller distortion),

cation position shifts (e.g., those associated with ferroelectricity), and/or octahedral tilting[27]. Driving forces for octahedral tilting, in particular, include the character of A-O and B-O bonding (covalency, orbital energy, width, and filling), repulsion between like ions, and ion size mismatch[28]. In the present case of LSGN, Jahn-Teller distortion, the nature of the A-O and B-O bonds, and the ion size ratio may influence the observed changes in symmetry as a function of Ni content, temperature, and oxygen partial pressure. The following discussion considers how each of these three factors may influence the observed changes in crystal symmetry.

Regarding octahedral distortions: it has been suggested, on the basis of electron paramagnetic resonance (EPR) measurements of the related compounds $LaSrGa_{1-x}Ni_xO_{4-\delta}$, that for low Ni contents, Ni^{3+} ions adopt the low spin state, within elongated NiO_6 octahedra, whereas higher Ni contents promote the high spin state as an electronic band is formed[29]. Similar EPR results for LSGN perovskites were interpreted as showing that when the overall Ni content increases, the fraction of magnetically interacting (vs. isolated) Ni^{3+} increases[23]. Again in this case the lower symmetry "isolated Ni" signal was indicative of Ni in distorted/elongated NiO_6 octahedra, consistent with low spin Ni^{3+}. Low spin Ni^{3+} (having 5 d electrons) exhibits more Jahn-Teller distortion than high spin Ni^{3+}, so on this basis one might expect more octahedral distortion to be present in NiO_6 octahedra in the oxidized, low Ni content, $x = 0.05$ sample than in the $x = 0.5$ sample. These octahedral distortions in the $x = 0.05$ sample may lower the overall symmetry at low temperatures and influence the magnitude of thermo-chemical expansion coefficients, since lowering the oxygen partial pressure or increasing the temperature lead to removal of the octahedral distortion, via reduction of Ni^{3+} to Ni^{2+} and/or a spin unpairing transition in Ni^{3+}. Nonetheless the overall concentration of Ni is low in this case, and the effect may be minor, in agreement with the higher symmetry observed for low Ni contents in figure 2c. (Also, it should be noted that, in contrast to the aforementioned reports, Ni^{3+} was demonstrated to take the low spin state in $LaNiO_3$[30], and other authors have pointed out a correlation between charge delocalization and the low spin state[31].) In addition to this potential influence of spin state on symmetry, spin state also affects the effective B-site cation radius and hence the magnitude of thermo-chemical expansion, as discussed later.

Regarding bonding: Woodward[28] has suggested that optimization of the first coordination sphere around A cations may drive octahedral tilting. In the present work, the creation of oxygen vacancies upon increasing Ni concentration, increasing temperature, and/or decreasing oxygen partial pressure changes the local environment around the A cation and is expected to influence the related octahedral tilting, leading to overall changes in symmetry, which may partially explain the behavior seen in fig. 2c. One expects the magnitude of such changes to increase with the concentration of oxygen vacancies so created. (Similarly, B-O bonding is also related to symmetry; deviation from the ideal cubic structure changes the B-O-B angle, which lessens the degree of B-O orbital overlap (for σ or π bonding), which, in turn is expected to result in a greater degree of B-cation charge localization[28]. Therefore, changes in symmetry during heating and/or reduction may influence the degree of charge localization and thus indirectly the expansion coefficients; however the overall concentration of Ni is thought to play a bigger role in controlling the electronic structure and related properties in this system, as demonstrated via electrical conductivity measurements[20].)

Regarding the ion size ratio: in a perfect cubic perovskite, the length of the face diagonal of the unit cell is √2 times the length of the side, or (as predicted from ionic radii)

$$r_A + r_X = \sqrt{2}(r_B + r_X) \qquad (6)$$

where r_A, r_B, and r_X represent the radii of the A cation (La, Sr), B cation (Ga, Ni), and anion (O, V_O), respectively. Deviations from the perfect cubic structure are expected when this ratio is not satisfied and can be described by the tolerance factor, t[32]:

$$t = \frac{r_A + r_X}{\sqrt{2}(r_B + r_X)} \qquad (7)$$

While a value of t = 1 has been associated with cubic structures, for 3-3 perovskites such as $LaGaO_3$, hexagonal structures ($P6_3cm$) exist for ~0.83 < t < 0.9 (when r_B is too large), orthorhombic distortions (Pnma, Pbnm) for 0.9 < t < 1 (when r_B is slightly too large), and rhombohedral or hexagonal structures (R-3c) for t > 1 (when r_B is too small)[33], though there are exceptions. In these less symmetric structures the non-ideal radii are accommodated by tilting and/or distortion of the BO_6 octahedra[34]; Sasaki has noted a correlation between

observed tolerance factor and octahedral tilt[35,36]. For the present composition of $La_{0.9}Sr_{0.1}Ga_{1-x}Ni_xO_{3-\delta}$, the various radii can be expressed as:

$$r_A = 0.9r_{La} + 0.1r_{Sr}$$

$$r_B = (1-x)r_{Ga} + xr_{Ni}$$

$$r_X = \left(1 - \frac{\delta}{3}\right) r_O + \frac{\delta}{3} r_V \qquad (8)$$

In LSGN, the average B site radius will change with addition of Ni, reduction of Ni, and/or change in Ni spin state[37] (r_{Ga} = 0.62 Å, $r_{Ni}^{3+,hs}$ = 0.6 Å, $r_{Ni}^{3+,ls}$ = 0.56 Å, r_{Ni}^{2+} = 0.69 Å). While it is not possible to calculate exact tolerance factors for LSGN without knowing the effective radius of an oxygen vacancy (calculated later), average spin state, nor the exact distribution of Ni^{3+}/Ni^{2+}, one can infer trends from consideration of the B-site radius and from the knowledge that $LaGaO_3$ is close to the ideal cubic structure ($t_{LaGaO3} \approx 0.97$).

Addition of Ni, largely in the 3+ state in air[16,23], in $La_{0.9}Sr_{0.1}Ga_{1-x}Ni_xO_{3-\delta}$ lowers r_B and increases t enough to change the structure from orthorhombic to rhombohedral; presumably then t > 1. (Note that, using the above-mentioned radii in eq. 7, for t > 1 in this case, the oxygen vacancy radius, r_V, must be slightly smaller than the oxide ion radius, r_O, as previously found for fluorite-structured oxides[10].) Conversely, isothermally lowering the oxygen partial pressure and thereby reducing the Ni valence state increases r_B and (potentially counterbalanced by $r_V < r_O$) is expected to decrease t from its larger rhombohedral value; if the effect is small, t would approach 1 and the symmetry would increase, as indeed is observed in figure 1. (Note that the spin state of Ni^{3+} will affect the magnitude of this change: high spin Ni^{3+}, having a larger radius, will expand less upon reduction than low spin Ni^{3+}.) Increasing temperature reduces the Ni and may increase the Ni spin state, both of which increase r_B and (again possibly counteracted by slight changes in r_X) decrease t, increasing the symmetry for small changes. Beyond these considerations of individual radius changes, one expects the overall increase in bond lengths and importance of entropic changes with increasing thermal energy to also influence structural changes with increasing temperature. Thus a variety of phase transitions upon heating, consisting of decreases in octahedral tilting and changes in octahedral size and shape, have

been reported for other perovskites[38,39], even in the absence of significant spin state and point defect contributions discussed above. Similar to the present work, these reports demonstrate an increase in symmetry with increasing temperature.

Overall the XRD study here suggests that thermo-chemical expansion in LSGN increases the crystal symmetry. The behavior is consistent with expected changes in ionic radii, but as described above, changes in octahedral distortions (via spin state changes) and bonding environments may also contribute to symmetry changes. Further high resolution XRD or neutron diffraction studies of chemical expansion in perovskites, yielding atomic coordinates over a wider range of oxygen stoichiometries, would shed more light on these processes.

Origins of Chemical Expansion

From the thermogravimetric and dilatometric measurements, the primary observation is that, while increasing the Ni concentration increases the magnitude of oxygen stoichiometry changes and expansion over a given oxygen partial pressure range, the value of the CCE (expansion normalized to change in stoichiometry) is lowered. This result is consistent with our prior DFT predictions suggesting that decreased charge localization (manipulated in this case by Ni content) decreases the CCE[12]. In the DFT calculations the lower CCE was attributed specifically to a smaller radius of the reduced B-site cation (Ce^{3+}) by 4% owing to the charge delocalization. From the experimentally measured CCEs in the present study it is possible to estimate the reduced B-site cation radius (Ni^{2+}) in the "delocalized" (x = 0.5) case and compare it to the "localized" (x = 0.05) case. This calculation employs recently derived equations (derivation given in ref. [40]) relating the chemical expansion of perovskites to their constituent radii, with coefficients *A* and *B* obtained from fitting a wide range of perovskite oxides:

$$r_V = \frac{3\alpha_V a_0}{\left(\frac{A}{\sqrt{2}}+B\right)} + r_O \qquad (9)$$

$$\alpha_V = \alpha_C - \frac{2}{x}\alpha_B \qquad (10)$$

$$\alpha_B = \frac{B}{a_0} x\left(r_{B(red)} - r_{B(ox)}\right) \qquad (11)$$

where a_0 is the pseudo-cubic lattice parameter in the initial state (prior to reduction, e.g., for all Ni in the 3+ state), A = 0.491, B = 2.005, $r_{B(red)}$ and $r_{B(ox)}$ are the radii of the reduced and oxidized multivalent B-site cation (Ni^{2+} and Ni^{3+}, respectively, in this case), α_B represents a contribution to the chemical expansion coefficient resulting from the change in B-site radius, and the other variables (measured chemical expansion coefficient α_C, vacancy radius r_V, oxide ion radius r_O, and Ni content x) have already been introduced.

First the oxygen vacancy radius was determined from Eq. 9 after substituting Eqs. 10 and 11 for α_V and α_B, respectively, and using the measured chemical expansion coefficient in the charge localized (x = 0.05) case along with relevant Shannon ionic radii. Then, using that oxygen vacancy radius, which was assumed to be independent of Ni content, the term ($r_{B(red)} - r_{B(ox)}$) was determined for the charge delocalized (x = 0.5) case, again using eqs. 9-11. One may then estimate the radius of the reduced cation (Ni^{2+}) with delocalized behavior, using the Shannon radius for the oxidized cation (Ni^{3+}). The resulting radii are given in Table II.

Table II: Oxygen vacancy radius, r_V, calculated from the measured CCE for x = 0.05, and effective Ni^{2+} radius calculated from the measured CCE for x = 0.5, as described in the text.

T, °C	**Assumed spin state for Ni^{3+} in both compositions**	**x = 0.05**		**x = 0.5**
		r_V, Å	**$\frac{r_V}{r_O}$**	**$\frac{r}{r_{ionic}}$ for Ni^{2+}**
800	low	0.93	0.66	0.998
	high	1.13	0.81	0.997
900	low	0.97	0.70	0.989
	high	1.18	0.84	0.989

First, one notes that the oxygen vacancy radius is smaller than the oxide ion radius, in agreement with our prior findings of lattice relaxations around vacancies in fluorite-structured oxides[10] and with very recent calculations for the Sr- and Mg-doped $LaGaO_3$ perovskite[41]. Second, at 800 °C the calculated Ni^{2+} radius decreased 0.2-0.3 %, and at 900 °C the calculated Ni^{2+} radius decreased 1.1 % for the x = 0.5 case compared to the x = 0.05 case. These values, while limited by the assumptions inherent in the calculations, are consistent with the occurrence of charge delocalization, but they are not as large as the multivalent cation radius change reported by DFT calculations on Ce-containing oxides (~4%). Similarly, the magnitude of the *overall* change in CCE in the present work (~5-20%) is much smaller than that obtained in Ce systems by the previous theoretical calculations (>70%).

Several factors could be responsible for this discrepancy: 1) the change in extent of charge localization may be smaller in the present work; 2) the multivalent cation is smaller in this work[37]; 3) the spatial distribution and symmetry of the wave functions is different in this work (4f in Ce and 3d (with 2p admixture from O) in Ni); 4) other factors, such as the complex structural changes observed by XRD, likely contribute to the overall measured chemical expansion in perovskites. For example, the locally anisotropic expansion accompanying the increase in symmetry may influence the macroscopic expansion coefficients. The dilatometric measurements of expansion represent an average over many grains of different orientations in the polycrystalline bulk samples; in addition, stress generation owing to differential expansion in adjacent grains of different orientations could limit the extent of the expansion in anisotropic samples. A significant effect of anisotropy has been reported for layered oxygen hyperstoichiometric K_2NiF_4-type structures, where the macroscopic chemical expansion coefficient of polycrystalline samples is small, owing to different chemical expansion coefficients along the a- and c-directions[42], although in that case expansion along one crystallographic axis is balanced by shrinkage along the other. In the present work, the more anisotropic expansion observed in the sample with higher Ni content (x = 0.5) could be one factor contributing to a lower macroscopic chemical expansion coefficient vs. x = 0.05. If significant, this effect also suggests that one may observe a greater influence of charge delocalization on macroscopic CCEs in cubic perovskites compared to

the distorted perovskites in the present work. Further work to investigate the relative importance of different factors controlling chemical expansion in perovskites is therefore warranted.

Along those lines, Frade[43] has demonstrated a correlation between increased tolerance factor (after reduction) and increased CCE for some perovskite-structured mixed ionic and electronic conductors with $t < 1$, implying larger chemical expansion coefficients when the cubic perovskite phase becomes more stable ($t \rightarrow 1$) upon reduction. In the present work the XRD results suggest that at high temperatures the structures appear to be quite similar for low and high Ni contents (figs. 1 and 2). The decrease in CCE with increasing [Ni] in this work therefore might not be explained by this reported correlation of CCE and t. Nonetheless, a similar trend in CCE vs. multivalent cation concentration to the present work has been observed previously[44] in $La_{0.3}Sr_{0.7}Ga_{1-x}Fe_xO_{3-\delta}$, where the CCE at 800 °C was ~23% lower for x = 1 vs. 0.6. In that work the authors suggested that substitution of a fixed valent B-site cation (e.g., Ga) in place of the multivalent cation (e.g., Fe) induced disorder, which increased the CCE. In the LSGF system the role of charge delocalization vs. Fe concentration may not be so pronounced compared to the present work with Ni, since conduction in Fe-containing perovskites appears largely to be polaronic, even for high Fe concentrations[45,46]. Also, in the present case, the maximum amount of the multivalent cation, Ni, is lower and thus ordering is not, to a first approximation, expected to be as significant.

One final consideration for the LSGN system returns to the role of spin state and its effect on the Ni^{3+} radius. One would expect a slightly smaller radius expansion upon reduction of Ni^{3+} to Ni^{2+} and a significantly lower chemical expansion coefficient when high spin Ni^{3+} is present (suggested for high overall Ni concentrations[23,29]) compared to one where Ni^{3+} is in the low spin state (suggested for low overall Ni concentrations at room temperature[23,29]), as is indeed observed in this work. Such an effect may complement the influence of charge delocalization in lowering the chemical expansion coefficient with increases in Ni content, although the Ni^{3+} spin state vs. Ni concentration has not been characterized at elevated temperatures. Owing to the unknown influence of composition on spin state in the temperature range of interest, and the inapplicability of Shannon radii for the delocalized charge case, it is difficult to calculate how large of an

effect any differences in spin state have upon the measured CCEs in the present work. In future work, studies isolating each of these possible contributors to chemical expansion would be beneficial.

Experimental Approach

Bulk (~20 mm x 3 mm x 3 mm), bar-shaped specimens of $La_{0.9}Sr_{0.1}Ga_{1-x}Ni_xO_{3-\delta}$, x = 0.05, 0.1, 0.5, were fabricated from powders prepared by the Pechini method, followed by pressing and sintering in air at 1400 °C, as described in more detail previously[22]. *Ex situ* phase purity of the resulting samples was examined by X-ray diffraction (XRD) using a PANalytical X'pert Pro Multipurpose Diffractometer (PANalytical Inc., Westborough, MA, USA) with Cu Kα radiation, a step size of ~0.02°, a current of 40 mA and voltage of 45 kV. *In situ* studies of the crystallographic structure, as a function of temperature (600-900 °C) and oxygen partial pressure (pO_2 = 0.21 atm, 10^{-3} atm), were evaluated on the same instrument, for the x = 0.05 and x = 0.5 compositions, with an Anton Paar HTK 1200N furnace attachment and pre-mixed N_2/O_2 gases. XRD measurements were made first at pO_2 = 0.21 atm, with increasing temperature steps after holding at each temperature to equilibrate the sample (required holding times were determined from the measured equilibration times during thermogravimetric measurements, described below), cooled to room temperature to check reversibility, then repeated with the same temperature profile at $pO_2 = 10^{-3}$ atm. Oxygen partial pressure was verified with an external ZrO_2-based Nernst-type sensor. Profile fitting of the XRD data for phase identification and lattice parameter determination was performed using the programs HighScore Plus (PANalytical, Inc.) and JADE 9 (Materials Data, Inc.).

CCEs were determined from equation 1 by isothermal measurements of non-stoichiometry changes (Δδ) using thermogravimetric analysis (TGA) and of expansion (ε_C) using dilatometry over the same oxygen partial pressure range (1atm – 10^{-3}atm). In this calculation, the ε vs. pO_2 data were interpolated using a quadratic function in order to calculate equivalent ε values corresponding to the same pO_2 values used in the TGA measurements. For TGA of mass changes in different oxygen partial pressures, the sample was suspended from an XP6 microbalance (Mettler-Toledo K.K., Tokyo, Japan) by Pt wire in a vertical tube furnace. Gas flow (200 sccm total, N_2/O_2 mixtures) was set using mass flow controllers and measured with

an *in situ* Y_2O_3-stabilized ZrO_2 Nernst-type electromotive force sensor; temperature was monitored by an S-type thermocouple placed close to the sample. The change in oxygen stoichiometry was calculated from the measured mass changes using the following equation:

$$\Delta\delta = \frac{mol\ O\ lost}{mol\ LSGN} = \frac{-(m-m_{ref})/M_O}{mol\ LSGN} \qquad (4)$$

where m is the sample mass (in g), m_{ref} is the mass of the sample in the reference condition (air at the temperature of interest), M_O is the mass of one mole of atomic oxygen (15.9995g), and "mol LSGN" is the number of moles of $La_{0.9}Sr_{0.1}Ga_{1-x}Ni_xO_{3-\delta}$ in the specimen, approximated from the initial sample mass at room temperature in air. The Al_2O_3 push-rod dilatometer was custom-built, with the same control and *in situ* monitoring of gas flow, oxygen partial pressure, and temperature as in the TGA setup. The expansion (ε) was determined from the measured change in dilatometer position as:

$$\varepsilon = \Delta l/l_0 = (p - p_{ref})/l_0 \qquad (5)$$

where p is the dilatometer sensor position relative to a reference point (p_{ref}, taken in air at the temperature of interest), Δl is the change in specimen length determined from the dilatometer position, and l_0 is the initial length measured at room temperature in air. Use of l_0 instead of the actual specimen reference length at the high temperature reference point (at p_{ref}) results in very small error in the expansion calculation (<~1%). Both the thermogravimetric and dilatometric measurements were performed in small, decreasing increments of oxygen partial pressure, then repeated in increasing oxygen partial pressure steps to check for reversibility. Time-dependent drift in the dilatometric measurements was observed; the rate appeared to be constant regardless of specimen, so it is believed to originate in the instrument. This drift contribution was subtracted from the data. Additionally, at the highest temperatures and lowest oxygen partial pressures, slight irreversible weight loss was observed in the TGA measurements, which may be caused by Ga volatilization from the sample surface. Ga depletion at LSGN surfaces after sintering has been observed by other researchers[23].

Conclusions

The chemical expansion behavior of $La_{0.9}Sr_{0.1}Ga_{1-x}Ni_xO_{3-\delta}$ (LSGN) was studied experimentally to test theoretical predictions of decreased chemical expansion coefficient of oxides upon decreasing charge localization on multivalent cations. Prior electrical conductivity results demonstrated a transition from ionic, to localized electronic hopping, to metallic conduction with increasing Ni content, pointing to a corresponding charge delocalization with increasing Ni content. The structural changes accompanying thermo-chemical expansion were studied by *in situ* X-ray diffraction, whereas thermogravimetric analysis and dilatometry provided quantitative measures of the macroscopic chemical expansion accompanying oxygen stoichiometry changes for x = 0.05, 0.1, and 0.5. The XRD results showed that addition of Ni (above x = 0.05) caused a phase transition from orthorhombic to rhombohedral symmetry at room temperature, while even the x = 0.05 samples were rhombohedral at elevated temperatures. Increasing the temperature and/or decreasing the oxygen partial pressure increased the symmetry of the samples, with the x = 0.5 sample appearing almost cubic at 900 °C and $pO_2 = 10^{-3}$ atm. Correspondingly, the thermo-chemical expansion was anisotropic. The structural changes were consistent with expected tolerance factor changes, considering the B-site cation and oxygen vacancy radii, and with possible changes in bonding environment and Jahn-Teller distortions. Increasing the Ni content in LSGN gave rise to larger changes in oxygen stoichiometry and chemical expansion over a given oxygen partial pressure range, but to lower chemical expansion coefficients. The results are qualitatively consistent with the theoretical predictions, but the smaller measured magnitude of the effect in this materials system suggests that other inter-related factors, such as spin state changes, structural changes including anisotropic expansion, disorder, and the nature of the B-site cation, likely contribute as well to the chemical expansion behavior of perovskites. Finally, an effective radius of the oxygen vacancy was derived (see table 2), which was smaller than that of an oxide ion and in agreement with prior studies on fluorite-structured oxides.

Acknowledgements

The authors gratefully acknowledge L. Zhao (Kyushu University) for assistance with sample preparation and preliminary measurements by J. E. Thomas (MIT). NHP and SRB recognize partial support from WPI-I^2CNER, supported by the World Premier International Research Initiative (WPI), MEXT, Japan. HLT thanks the Department of Energy, Basic Energy Sciences, for support under award DE SC0002633.

Supplementary Material

Data from dilatometric and thermogravimetric measurements at 700 °C and 900 °C (expansion vs. oxygen partial pressure and change in non-stoichiometry vs. oxygen partial pressure), used to determine the chemical expansion coefficients given in table 1, are presented as supplementary material.

References

[1] S.R. Bishop, D. Marrocchelli, C. Chatzichristodoulou, N.H. Perry, M.B. Mogensen, H.L. Tuller, and E.D. Wachsman, "Chemical Expansion: Implications for Electrochemical Energy Storage and Conversion Devices," *Annual Review of Materials Research* 44 (2014) 6.1-6.35 (doi: 10.1146/annurev-matsci-070813-113329)

[2] S. B. Adler, "Chemical expansivity of electrochemical ceramics," *J. Am. Ceram. Soc.*, 84, 2117-2119 (2001)

[3] G. Mogensen and M. Mogensen, "Reduction reactions in doped ceria ceramics studied by dilatometry," *Thermochim. Acta.*, 214, 47 (1993)

[4] S.B. Adler, "Factors governing oxygen reduction in solid oxide fuel cell electrodes," Chemical Reviews 104 (2004) 4791-4843

[5] A. Atkinson, "Chemically-induced stresses in gadolinium-doped ceria solid oxide fuel cell electrolytes," *Solid State Ionics* 95 [3-4] (1997) 249-258

[6] R. Krishnamurthy and B.W. Sheldon, "Stresses due to oxygen potential gradients in non-stoichiometric oxides," *Acta Materialia* 52 [7] (2004) 1807-1822

[7] C. Chatzichristodoulou, M. Søgaard, and P.V. Hendriksen, "Oxygen Permeation in Thin, Dense $Ce_{0.9}Gd_{0.1}O_{1.95-\delta}$ Membranes I. Model Study," J. Electrochem. Soc. 158 [5] (2011) F61-F72

[8] K. Sato, T. Hashida, K. Yashiro, H. Yugami, T. Kawada, and J. Mizusaki, "Mechanical damage evaluation of solid oxide fuel cells under simulated operating conditions," *Journal of the Ceramic Society of Japan* 113 [1320] (2005) 562-564

[9] P.V. Hendriksen, J.R. Høgsberg, A.M. Kjeldsen, B.F. Sørensen, and H.G. Pedersen, in Advances in Solid Oxide Fuel Cells II, Ceramic Engineering and Science Proceedings, A. Wereszczak, Editor, v. 27, Cocoa Beach, USA (2007).

[10] D. Marrocchelli, S.R. Bishop, H.L. Tuller, and B. Yildiz, "Understanding chemical expansion in non-stoichiometric oxides: ceria and zirconia case studies," *Advanced Functional Materials* 22 [9] (2012) 1958-1965

[11] D. Marrocchelli, S.R. Bishop, and J. Kilner, "Chemical expansion and its dependence on the host cation radius," *Journal of Materials Chemistry A*, 1 [26] (2013) 7637-7680

[12] D. Marrocchelli, S. R. Bishop, H. L. Tuller, G. W. Watson, and B. Yildiz, "Charge localization increases chemical expansion in cerium-based oxides," *Physical Chemistry Chemical Physics*, 14, 12070-12074 (2012).

[13] H.L. Tuller and A.S. Nowick, "Small polaron electron transport in reduced CeO_2 single crystals," *J. Phys. Chem. Solids* 38 [8] (1977) 859-867

[14] N. Bonanos, "Transport properties and conduction mechanism in high-temperature protonic conductors," *Solid State Ionics* 53-56 (1992) 967-974

[15] F. Lecarpentier, H.L. Tuller, and N.J. Long, "Performance of $La_{0.9}Sr_{0.1}Ga_{0.5}Ni_{0.5}O_3$ as a Cathode for a Lanthanum Gallate Fuel Cell," *J. Electroceram.* 5 [3] (2000) 225-229

[16] J.-N. Audinot, J.-M. Bassat, A. Wattiaux, J.-C. Grenier, and M. Pouchard, "Investigations of the $LaGa_{1-x}Ni_xO_{3-\delta}$ ($x \leq 0.50$) system in the scope of SOFC's: synthesis and physical characterizations," *C.R. Acad. Sci. Paris*, t. 2, Serie II c, p.69-73 (1999)

[17] A.A. Yaremchenko, V.V. Kharton, A.P. Viskup, E.N. Naumovich, N.M. Lapchuk, and V.N. Tikhonovich, "Oxygen Ionic and Electronic Transport in $LaGa_{1-x}Ni_xO_{3-\delta}$ Perovskites," *Journal of Solid State Chemistry* 142 (1999) 325-335

[18] E.D. Politova, S. Yu. Stefanovich, A.K. Avetisov, V.V. Aleksandrovskii, T. Yu. Glavatskih, N.V. Golubko, G.M. Kaleva, A.S. Mosunov, and N.U. Venskovskii, "Processing, structure, microstructure, and transport properties of the oxygen-conducting ceramics (La,Sr)(Ga,M)O_y (M=Mg, Fe, Ni)," *J. Solid State Electrochem.* 8 (2004) 655-660

[19] L. Sebastian, A.K. Shukla, and J. Gopalakrishnan, "$La_{0.9}Sr_{0.1}Ga_{0.8}M_{0.2}O_{3-\delta}$ (M = Mn, Co, Ni, Cu or Zn): Transition metal-substituted derivatives of lanthanum-strontium-gallium-magnesium (LSGM) perovskite oxide ion conductor," *Bull. Mater. Sci.* 23 [3] (2000) 169-173

[20] N.J. Long, F. Lecarpentier, and H.L. Tuller, "Structure and electrical properties of Ni-substituted lanthanum gallate perovskites," *Journal of Electroceramics*, 3 (4), 399-407 (1999).

[21] G.Y. Gou, I. Grinberg, A.M. Rappe, and J.M. Rondinelli, "Lattice normal modes and electronic properties of the correlated metal $LaNiO_3$," *Phys Rev B* 84 (2011) 144101
[22] N.H. Perry, J.E. Thomas, D. Marrocchelli, S.R. Bishop, and H.L. Tuller, "Isolating the Role of Charge Localization in Chemical Expansion: (La,Sr)(Ga,Ni)O_{3-x} Case Study," *ECS Transactions*, v. 57, no. 1, pgs. 1879-1884 (2013)
[23] M.T. Colomer and J.A. Kilner, "Ni-doped lanthanum gallate perovskites: Synthesis and structural, microstructural, and electrical characterization," *Solid State Ionics* 182 (2011) 76-81
[24] Y. Wang, X. Liu, G.-D. Yao, R.C. Liebermann, and M. Dudley, "High temperature transmission electron microscopy and X-ray diffraction studies of twinning and the phase transition at 145 °C in $LaGaO_3$," *Materials Science and Engineering A* 132 (1991) 13-21
[25] X. Chen and T. Grande, "Anisotropic and Nonlinear Thermal and Chemical Expansion of $La_{1-x}Sr_xFeO_{3-\delta}$ (x = 0.3, 0.4, 0.5) Perovskite Materials," *Chemistry of Materials* 25 (2013) 3296−3306
[26] X. Chen and T. Grande, "Anisotropic Chemical Expansion of $La_{1-x}Sr_xCoO_{3-\delta}$," *Chemistry of Materials* 25 (2013) 927-934.
[27] P.M. Woodward, "Octahedral Tilting in Perovskites. I. Geometrical Considerations," *Acta Cryst.* B53 (1997) 32-43.
[28] P.M. Woodward, "Octahedral Tilting in Perovskites. II. Structure Stabilizing Forces," *Acta Cryst.* B53 (1997) 44-66.
[29] D. Reinen, U. Kesper, and D. Belder, "Mixed valent nickel and manganese oxide ceramics – model systems with superconducting properties?" *J. Solid State Chem.* 116 (1995) 355-363
[30] G. Demazeau, A. Marbeuf, M. Pouchard, P. Hagenmuller, and J.B. Goodenough, "Synthesis, Structure, and Magnetic Susceptibility of New Family of Oxygenated Nickel (III) Compounds," *Comptes Rendus Hebdomadaires des Seances de L'Academie des Sciences Serie C*, 272 [26] (1971) 2163-&
[31] C.N.R. Rao, O.M. Parkash, and P. Ganguly, "Electronic and Magnetic Properties of $LaNi_{1-x}Co_xO_3$, $LaCo_{1-x}Fe_xO_3$ and $LaNi_{1-x}Fe_xO_3$," *J. Solid State Chem.* 15 (1975) 186-192
[32] V.M. Goldschmidt, "Die Gesetze der Krystallochemie," *Die Naturwissenschaften* 21 (1926) 477–485.
[33] Mark Levy, "Crystal Structure and Defect Properties in Ceramic Materials," Imperial College London thesis (2005)
[34] M. Ahtee and L. Unonius, "The Structure of $NaTaO_3$ by X-ray Powder Diffraction," *Acta Cryst.* A33 (1977) 150-154
[35] S. Sasaki, CT Prewitt, and RC Liebermann, "The crystal structure of $CaGeO_3$ perovskite and the crystal chemistry of the $GdFeO_3$-type perovskites," *American Mineralogist* 68 (1983) 1189-1198
[36] S. Sasaki, CT Prewitt, JD Bass, and WA Schulze, "Orthorhombic perovskite $CaTiO_3$ and $CdTiO_3$ – Structure and space group," *Acta Crystallographica Section C – Crystal Structure Communications* 43 (1987) 1668-1674
[37] R.D. Shannon, "Revised Effective Ionic Radii and Systematic Studies of Interatomic Distances in Halides and Chalcogenides", *Acta Cryst.* A32 751-767 (1976).
[38] H.F. Kay and P.C. Bailey, "Structure and properties of $CaTiO_3$," *Acta Crystallographica* 10 (1957) 219-226
[39] C.N.W. Darlington and K.S. Knight, "High-temperature phases of $NaNbO_3$ and $NaTaO_3$," *Acta Crystallographica Section B – Structural Science* 55 (1999) 24-30
[40] D. Marrocchelli, N.H. Perry, and S.R. Bishop, "Understanding chemical expansion in perovskite-structured materials," (in preparation)
[41] C. Chatzichristodoulou, P. Norby, P. V. Hendriksen, and Mogens B. Mogensen, "Size of oxide vacancies in fluorite and perovskite structured oxides," J. Electroceram. DOI 10.1007/s10832-014-9916-2"
[42] V.V. Kharton, A.V. Kovalevsky, M. Avdeev, E.V. Tsipis, M.V. Patrakeev, A.A. Yaremchenko, E.N. Naumovich, and J.R. Frade, "Chemically induced expansion of $La_2NiO_{4+\delta}$-based materials," *Chem. Mater.* 19 (2007) 2027–33
[43] J.R. Frade, "Challenges imposed by thermochemical expansion of solid state electrochemical materials," p. 95 in Solid Oxide Fuels Cells: Facts and Figures, J.T.S. Irvine and P. Connor, eds., Springer (2013)
[44] V.V. Kharton, A.A. Yaremchenko, M.V. Patrakeev, E.N. Naumovich, F.M.B. Marques, "Thermal and chemical induced expansion of $La_{0.3}Sr_{0.7}(Fe,Ga)O_{3-\delta}$ ceramics," *Journal of the European Ceramic Society* 23 (2003) 1417-26
[45] L.-W. Tai, M.M. Nasralla, H.U. Anderson, D.M. Sparlin, and S.R. Sehlin, "Structure and electrical properties of $La_{1-x}Sr_xCo_{1-y}Fe_yO_3$. Part 1. The system $La_{0.8}Sr_{0.2}Co_{1-y}Fe_yO_3$," *Solid State Ionics* 76 (1995) 259-271
[46] J. Mizusaki, T. Sasamoto, W.R. Cannon, and H.K. Bowen, "Electronic conductivity, Seebeck coefficient, and defect structure of $La_{1-x}Sr_xFeO_3$ (x = 0.1, 0.25)" *J. Am. Ceram. Soc.* 66 (1983) 247-252